J Mater Sci (2011) 46:3868–3882
DOI 10.1007/s10853-011-5308-z

Impact of the electrodeposition chemistry used for TSV filling on the microstructural and thermo-mechanical response of Cu

Chukwudi Okoro · Riet Labie · Kris Vanstreels · Alexis Franquet · Mario Gonzalez · Bart Vandevelde · Eric Beyne · Dirk Vandepitte · Bert Verlinden

Received: 31 August 2010 / Accepted: 19 January 2011 / Published online: 1 February 2011

Abstract In this study, the role of electrodeposition chemistry on thermo-mechanical behavior of different Cu-films is examined. For this study, three different Cu electrodeposition chemistries were analyzed using Time-of-Flight Secondary Ion Mass Spectroscopy (TOF-SIMS), Focused Ion Beam (FIB), Laser Scanning method, Electron Backscattered Diffraction, and the Nano-indentation techniques. It is found that the level of impurity in Cu-films, resulting from the used electrodeposition additives, has a significant impact on their microstructural and thermo-mechanical behavior. Cu-films having high impurity content showed residual stress levels that are three times higher than the less impure Cu-films. This implies that the use of such impure electrodeposition chemistry for the filling of TSVs will result in high residual stresses in the Cu–TSV, thus inducing higher stresses in Si, which could be a reliability concern. Therefore, the choice of the used electrodeposition chemistry for the filling of TSVs should not be limited only to the achievement of a void free Cu–TSV, as consideration ought to be given to their thermo-mechanical response.

C. Okoro (✉) · R. Labie · K. Vanstreels · A. Franquet · M. Gonzalez · B. Vandevelde · E. Beyne
IMEC, 75 Kapeldreef, B-3001 Leuven, Belgium
e-mail: chukwudi.okoro@student.kuleuven.be

C. Okoro · D. Vandepitte
Department of Mechanical Engineering, Katholieke Universiteit Leuven, Leuven, Belgium

B. Verlinden
Department of MTM, Katholieke Universiteit Leuven, Leuven, Belgium

Introduction

The filling of Cu in through-silicon-vias (TSV) for 3D stacking of chips is achieved by an electrodeposition process. However, the achievement of a void free Cu–TSV remains a challenge that the microelectronics industry has been keen on solving. In recent times, many articles have reported on the successful void free filling of high-aspect ratio TSVs [1–9]. This break-through has been due to the gained fundamental understanding of the electrodeposition process and the role of the electrodeposition bath composition, in particular, the influence of the additives, in the filling of TSVs with Cu [4]. Today many vendors are selling Cu electrodeposition solutions that yield a void free Cu–TSV.

However, up till now, no thought has been given to the possible impact of the used additives on the thermo-mechanical behavior of Cu–TSVs. It is anticipated that the used additives, which acts as impurities, may have an impact on the microstructural behavior of the filled Cu, as back-end-of-line (BEOL) Cu studies have shown [10]. Therefore, as these Cu–TSVs are subjected to different thermal loads during their processing lifetime, their material properties will indeed impact on their thermo-mechanical response. This may in turn have an effect on the performance of the surrounding integrated devices [11–13] and the BEOL structure [14–16]. Therefore, the consideration for the choice of the used Cu electrodeposition solution should not be limited only to the achievement of a void free Cu–TSV but also the thermo-mechanical response of such material should be adjudged.

This article focuses on understanding the interaction between the used electrodeposition chemistry (i.e., the additives) and the thermo-mechanical behavior of different electrodeposited Cu. Since the size and geometry of

Cu–TSV makes it complex to characterize their thermo-mechanical and microstructural behavior, an approximation study is required. For this purpose, blanket Cu-films on silicon substrate were used. In this study, Time-of-Flight Secondary Ion Mass Spectroscopy (TOF-SIMS), Focused Ion Beam (FIB), the Laser Scanning method, Electron Backscattered Diffraction (EBSD), and the Nano-indentation techniques were the used analysis tools.

Tested materials and experimental procedure

For this study three films were studied.

Material 1

This is a commercial three component electrodeposition chemistry used for the filling of TSVs. This means that the electrodeposition bath chemistry contains accelerators (they *increase* the copper deposition rate), suppressors (they *decrease* the copper deposition rate), and levellers (they adsorb at the end of via filling process and avoid the formation of bumps) [4]. The details of the composition of the used additives are not known, as it is a proprietary secret of the manufacturer.

Material 2

This is a homemade three component electrodeposition chemistry model used for the achievement of a void free Cu–TSV. The Material 2 is a chloride containing copper sulfate electrolyte having disodium bis(3-sulfopropyl) disulfide, (S(CH2)3SO3Na)2, often called SPS, as an accelerator, polyethylene glycol (PEG MW 8000) as suppressor, and Janus Green B (JGB) as a leveller [1–4].

Material 3

This is a two component plating additive chemistry consisting of suppressors and accelerators, which is used for the BEOL metallization as well as for the formation of bond pads used for the achievement of Cu–Cu bonds.

For this experiment, a target uniform Cu-film of about 5 μm thick is electroplated on a full thickness silicon wafer (720 μm). The Cu-film thickness choice is based on the fact that the actual filled TSVs have a 5-μm diameter [7], [15], [16]. Afterward, the wafer was then diced to a size of 25 mm by 24 mm, as it is the required dimension for the used laser scanning method tool. The samples were then subjected to a repeated multiple thermal cycling (three times) between room temperature (RT) and a maximum temperature of 420 °C. The thermal cycling temperature is limited to 420 °C since it is the maximum temperature that the chip will ever undergo during its processing lifetime. Thereafter, the sample is additionally cycled from RT to 300 °C (twice). For this experiment, a heating/cooling rate of 5 °C/min is used. However, a cooling rate of 1 °C/min is used for temperature from 75 °C to RT since the tool cannot cool any faster at low temperatures. The used cycling profile is illustrated in Fig. 1.

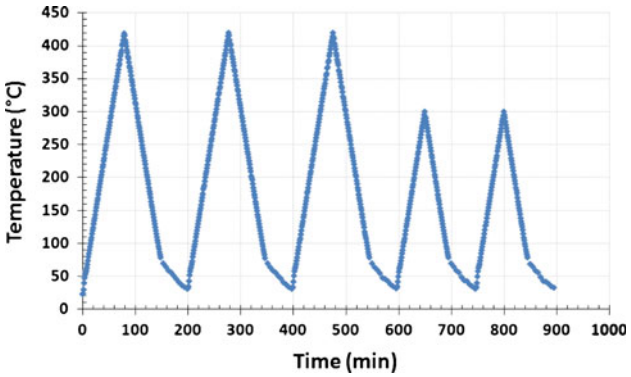

Fig. 1 The thermal cycling profile used for the determination of the thermo-mechanical behavior of Cu-films deposited using different electrodeposition chemistry baths

The choice of this temperature cycling profile is to determine how repeated thermal cycling affects the thermo-mechanical behavior of Cu. It will also inform us about how many cycles are required to achieve a stabilized Cu-film.

By measuring the change in wafer curvature ($1/R$) and using Stoney's equation represented in Eq. 1, the stress in thin films can be calculated as a function of temperature from

$$\sigma_f = \frac{M_s}{6}\frac{t_s^2}{t_f}\left(\frac{1}{R_1} - \frac{1}{R_2}\right) \tag{1}$$

where σ_f is the stress in the thin film, M_s is the biaxial modulus of the substrate, t_s and t_f are the substrate and film thickness, respectively, R_1 is the initial radius of curvature before film deposition or after film removal, R_2 is a measured radius curvature. For a single-crystal anisotropic material such as silicon, its biaxial modulus (M_s^{Si}) differs with its orientation. According to [17] the biaxial modulus, values for (001) and (111) silicon are given in Eqs. 1a and 1b, respectively.

$$M_s^{Si}(001) = 180.3\,\text{GPa} \tag{1a}$$

$$M_s^{Si}(111) = 229.1\,\text{GPa} \tag{1b}$$

After the laser scanning measurement has been completed on the bimaterial, the Cu-films were etched away using a mixture of H_2O_2 and $H_2{\cdot}SO_4$ (1:4). Thereafter the bare silicon substrate is measured alone and by the use of the Stoney equation the stress in the film is determined.

To ensure for good measurement, the reflected laser intensity is kept to an intensity of about 2000 counts, the measured data are acquired for every 5 min. More than three repetitions were performed for each of the three different electrodeposition Cu chemistries.

For a detailed interpretation of the thermo-mechanical response of the different Cu-films obtained from the laser scanning method, other supporting analytical tools were also used, which are TOF-SIMS, FIB, EBSD, and nano-indentation techniques. The TOF-SIMS is used to detect the impurities in the Cu-films, while FIB and EBSD tools are used to study the microstructural evolution of the films. On the other hand, the nano-indenter is used for the determination of the hardness and the elastic modulus of the different Cu-films. For these measurements, the samples were analyzed twice; *before* and *after* thermal cycling. Based on these additional studies, the laser scanning measurements results were interpreted. The results and discussions of these analyses are presented in the subsequent sections.

Measurement of Cu-film thickness

Since the calculation of the stress in the film is related to the film thickness as illustrated by the Stoney equation, it is important to quantify the thickness of the films as accurately as possible. For this purpose, a surface profilometry tool from Veeco Company called Wyco is used. It is a non-contact optical profiler system that uses two technologies to measure a wide range of surface heights; phase-shifting interferometry (PSI) mode, which allows for measurement of smooth surfaces and small steps, and vertical scanning interferometry (VSI) mode allows for the measurement of rough surfaces and steps up to several millimeters high. In both techniques, the light reflected from a reference mirror combines with light reflected from a sample to produce interference fringes, where the best-contrast fringe occurs at best focus [18].

Table 1 Thickness of the different Cu-films obtained using the Wyko surface profilometry technique

Samples	Flim thickness (μm)
Material 1	6.3 ± 0.4
Material 2	5.6 ± 0.5
Material 3	4.6 ± 0.3

To determine the deposited Cu-film thickness, a section of the blanket Cu-film is removed so as to reveal the silicon substrate. Using the Wyco tool, the surface profile across the etched surface is carried out. Thus, the correct thickness of the Cu-film is determined since it is the height difference between the etched region (substrate) and the top of the sample (Cu-film). The images of the surface profilometry measurement for the Material 1 Cu-film are shown in Fig. 2. From this measurement, the average values for the three different films are tabulated in Table 1. These values were used for the calculation of the stress in the Cu-films using the Stoney equation.

It is worth noting that for the achievement of good adhesion between Cu-film and its Si substrate, a 5 nm Ti/Cu seed layer is deposited before the electrodeposition of Cu-film. This also inhibits the diffusion of Cu in Si substrate. It is used extensively as a liner for the making of robust Cu–TSVs [2], [7], [15].

Results: laser scanning method

Material 1

Figure 3 shows the plot of the calculated biaxial stress versus temperature for the Material 1 chemistry based on the Stoney equation. From this plot, it could be observed that the stress in the film changes as a function of the applied temperature. These stresses arise due to the thermal strain built up in the film upon temperature excursion

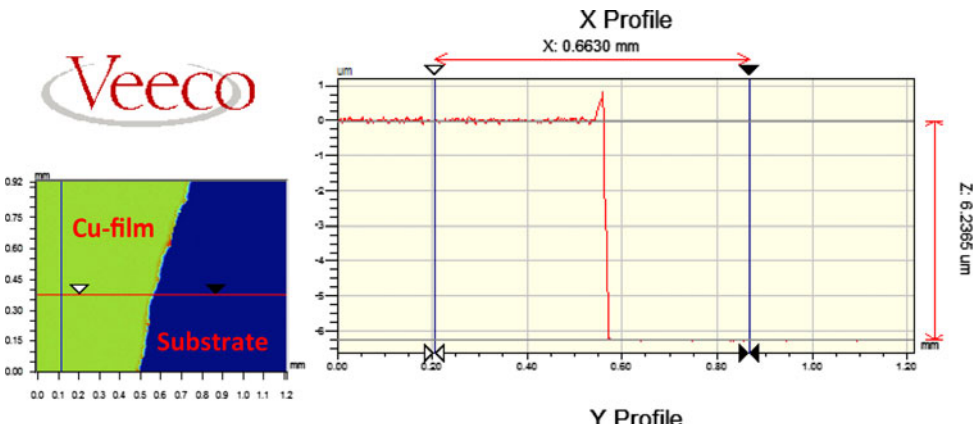

Fig. 2 Results from laser profilometry showing the images of the measured thicknesses of the Material 1 Cu-film samples

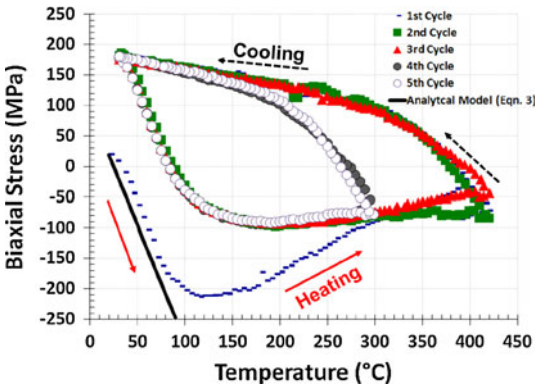

Fig. 3 Biaxial stress response of Material 1 Cu-film under thermal cycling

caused by the CTE mismatch between the Cu-film and the elastic Si substrate. The thermal strains results in thermal stress build up due to the constraint from free expansion imposed on the film by the much thicker Si substrate. In an elastic state, the thermal strain is given by

$$\varepsilon_e = \Delta\alpha\Delta T = (\alpha_f - \alpha_s)(T - T_0) \quad (2)$$

where ε_e is the elastic thermal strain in the film, α_f and α_s represent the CTE of the film and the substrate, respectively, T_0 and T, respectively, represent the initial temperature and the operating temperature. This means that the CTE of the substrate and the film is assumed to be constant. This elastic thermal strain in the film is related to the elastic thermal stress for a biaxial stress state by

$$\sigma_e = \left(\frac{E_f}{1 - \upsilon_f}\right)\varepsilon_e, \quad (3)$$

where σ_e, υ_f, and E_f are the elastic thermal stress, Poisson ratio, and the elastic modulus of the film, respectively.

Based on Eq. 3, the biaxial stress in the Cu-film could be calculated, as is shown in Fig. 3. A good prediction of the stress in the elastic region for the 1st cycle is achieved. The values used for this calculation are presented in Table 2. While the E_f is obtained from the nano-indentation measurement presented in Sect. Nano-indentation results of this article; its CTE is calculated from the slope of the elastic region using Eq. 4 below

$$k = \frac{d\sigma}{dT} = (\alpha_s - \alpha_f)\left(\frac{E_f}{1 - \upsilon_f}\right). \quad (4)$$

Therefore, during the initial heating process elastic thermal stresses are built up. At first a near linear relation between stress and temperature is noticed (Fig. 3) but after a particular value of ΔT, a non-linear behavior is observed, as the stress in the film begins to saturate. This evolution of stress in a film during thermal cycling is the result of two competing processes: development of elastic stresses from the thermal expansion mismatch between the film and the Si substrate, and stress relaxation by irreversible processes discussed later [19].

From this graph, it is observed that at the beginning of the test, the Cu-film had a residual stress of about 20 MPa. This is an intrinsic stress resulting from the deposition process. It is tensile at RT, but on heating it starts to become compressive. This is because of the constraint imposed by the substrate that has a lower CTE (2.3 ppm/°C) than Cu (16.7 ppm/°C) [20], hindering its free expansion on heating. When cooling down, the stress in the film is observed to become tensile, because the Cu-film is constrained by the Si substrate from contracting. Thus, the high tensile stress of 200 MPa, observed at RT at the end of each cycle, is caused by the CTE mismatch between the Cu-film and Si substrate resultant from the temperature change (ΔT).

The Cu-film is observed to deform elastically from RT till about 85 °C. Above 85 °C, the film deviates from linear behavior, suggesting that some microstructural changes are taking place [21]. Further temperature excursion is observed to result in a rapid decrease in the measured stress from −200 MPa at 100 °C to about −75 MPa at 325 °C. However, above 325 °C the drop in stress becomes minimal. During the cooling process, after the attainment of the maximum temperature of 420 °C, the stress in the Material 1 film starts to become tensile. A maximum tensile stress of about 200 MPa is attained at the end of the cycle, as the formation of a hysteresis is observed in each cycle. This observed hysteresis is because Cu is an elastic–plastic material, thus, it has both elastic and plastic components. The hysteresis loop represents the energy dissipated in the material within one cycle.

The 2nd and the 3rd thermal cycles that were also cycled to a maximum temperature of 420 °C, have a closed hysteresis loop that is similar both in shape, size and position, but very different from the initial cycle as could be seen in Fig. 3. This means that no further microstructural transformation occurs in the Cu-film after it has fully undergone the 1st thermal cycling, leading to a stabilized thermo-mechanical response of the film. It can also be observed that during heating after the 1st cycle that at a temperature of about 85 °C a change in the slope of the stress–temperature response is observed. Above this temperature no further increase in the stress magnitude above −90 MPa is observed. This means that at this stress level, the films yields, thus deforming plastically, as it cannot accommodate further increase in stress.

Table 2 Material 1 properties used in Eq. 3 for the calculation of elastic stress as shown in Fig. 3

CTE (ppm/°C)	E modulus (GPa)	Initial temp. (°C)	Poisson
22.8	121.0	25.0	0.35

Additional cycles—4 and 5th cycles show a much smaller hysteresis loop since their maximum excursion temperature (300 °C) is much lower than in the earlier cycles. Their loops are found to fit well within the loops of the preceding cycles that were heat treated to 420 °C as well as attaining the same maximum stress level, thus, lower maximum temperature excursion did not result in any change in the thermo-mechanical material behavior of the film.

Material 3

The Material 3 Cu-film is observed to exhibit similar elastic–plastic behavior as the Material 1 chemistry as illustrated in Fig. 4. The film is observed to have an initial residual stress of about 50 MPa and a maximum tensile stress of ~180 MPa. After the first thermal cycle, succeeding thermal cycles to 420 °C are all observed to have the same sharp, size and position, which infer that the subsequent thermal cycling stabilizes the Material 3 film. However, the difference between the Material 3 Cu-film and the Material 1 chemistry is observed in the cooling curve for cycles with a maximum excursion temperature of 420 °C. The Material 3 Cu-film showed less elastic recovery on cooling from 420 °C, as the slope of the cooling curve is observed to change after a temperature of about 390 °C. Thus, the film shows more elastic deformation during the heating stage than the cooling stage, giving rise to the asymmetric shape of the hysteresis loop, while for the Material 1 Cu-film, the elastic region for the heating and cooling stages are very comparable (see Fig. 3). However, for 4 and 5th thermal cycling to 300 °C show a much more symmetric hysteresis loop

Material 2

Figure 5 shows two different measurements of the Material 2 Cu-film. However, this film is observed to behave very

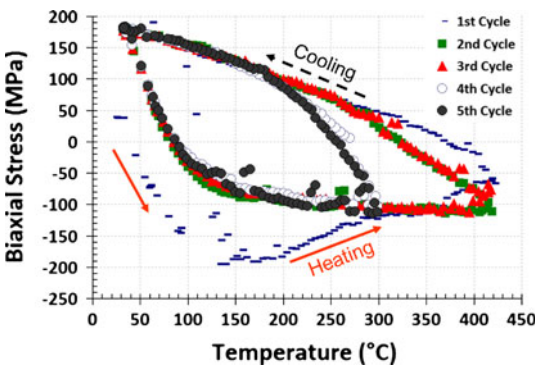

Fig. 4 The biaxial stress response of Material 3 Cu-film under thermal cycling

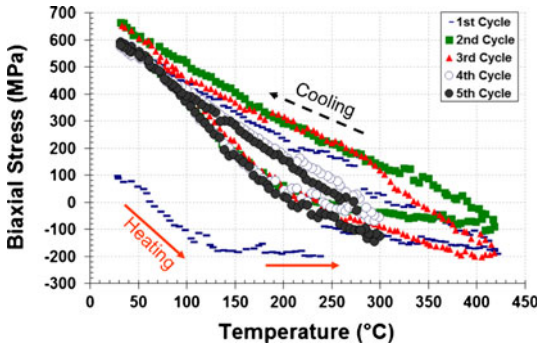

Fig. 5 The biaxial stress response of Material 2 under thermal cycling

differently from the other Cu-films; Material 1 and Material 3 Cu-film. High residual stress of about 100 MPa is observed in the film, with a maximum tensile stress *after* cycling of more than 650 MPa, which is more than three times larger than the aforementioned Cu-films.

Upon heating during the initial cycle, the Material 2 Cu-film is observed to behave similarly to that of the Material 1 and the Material 3 Cu-film, as the material response is observed to deviate from linearity after a temperature of about 100 °C, subsequently, a decrease in the attained stress is observed. However, the succeeding cycles are observed to be entirely differently from that of the other studied Cu-films both in shape and in size. These loops are very narrow with no distinct observed plastic deformation regime. Since the area in the hysteresis loop represents the energy dissipated by a material, thus, the observed smaller hysteresis loop infers that the Material 2 exhibits much more of an elastic response. Also, it can be observed that the film only stabilises after its second thermal cycling, as the second cycle is observed to have an open loop just as its first cycle, thus, it has a more unstable thermo-mechanical behavior in comparison to the afore studied films. However, the reason for this difference in thermo-mechanical behavior cannot be explained from the presented stress–temperature curves, thus, different experiments were performed which are presented in the subsequent sections, followed by a discussion that explains this peculiar film behavior.

TOF-SIMS analysis

The TOF-SIMS analysis of the Material 1, Material 2, and the Material 3 Cu-films were analyzed. First, the analysis was performed for a sample without thermal cycling, and a second analysis was performed after the sample has been thermally cycled using the thermal cycling profile shown in Fig. 1. For this study, the incorporation of different elements such as nitrogen, carbon, sulfur, fluorine, chlorine,

and oxygen in the different films resulting from the deposition additives were studied. All these studied elements were detected directly except for nitrogen which was detected by measuring the cyanide (CN^-) fragments [4]. This is because the ionization yield of nitrogen is very low, thus could only be detected as a CN^- cluster. A plot of the intensity as a function of the sputter time is presented in Figs. 6 and 7 for all the three studied Cu-films.

The profiles show that the intensity of the different elements initially decreases with respect to the sputter time, thereafter, it is observed to saturate. This observed steep decline is because the surfaces of the Cu-films are exposed to air leading to their contamination, which is removed by sputtering. As the surface contamination is very thin, it is quickly removed, resulting in a steep decrease of their intensities. This means that for the interpretation of the curves, the saturated region of the graph shows the correct intensity of the analyzed elements.

From Figs. 6 and 7, it can be observed that all three tested Cu-films showed very negligible sulfur and fluorine contaminants content both *before* and *after* thermal cycling, since the intensity counts were about 1 count/s. In addition, a marginal content of nitrogen and chlorine impurities of less than 3 counts/s are observed for the Material 3 and the Material 1 Cu-films both *before* and *after* thermal cycling. These two Cu-films are observed to show much similarity in their impurity content even though the Material 1 is three component chemistry, thus contains an extra additive (leveler), than the Material 3 Cu-film which is two component chemistry, having less additives in its electrodeposition chemistry bath.

Unlike the other Cu-films, the Material 2 chemistry is observed to have very high impurity content of chlorine and CN. The intensity of the chlorine content *before* thermal cycling (Fig. 6c) is about 1400 counts/s, while the CN content *before* thermal cycling is about 480 counts/s. However, *after* thermal cycling it is observed that the intensity of chlorine and nitrogen reduces to 1100 and 430 counts/s, respectively. This indicates that during the thermal cycling process that part of the plating chemistry additives is lost due to their decomposition which may lead to the out-gassing of some of its constituents, thus resulting

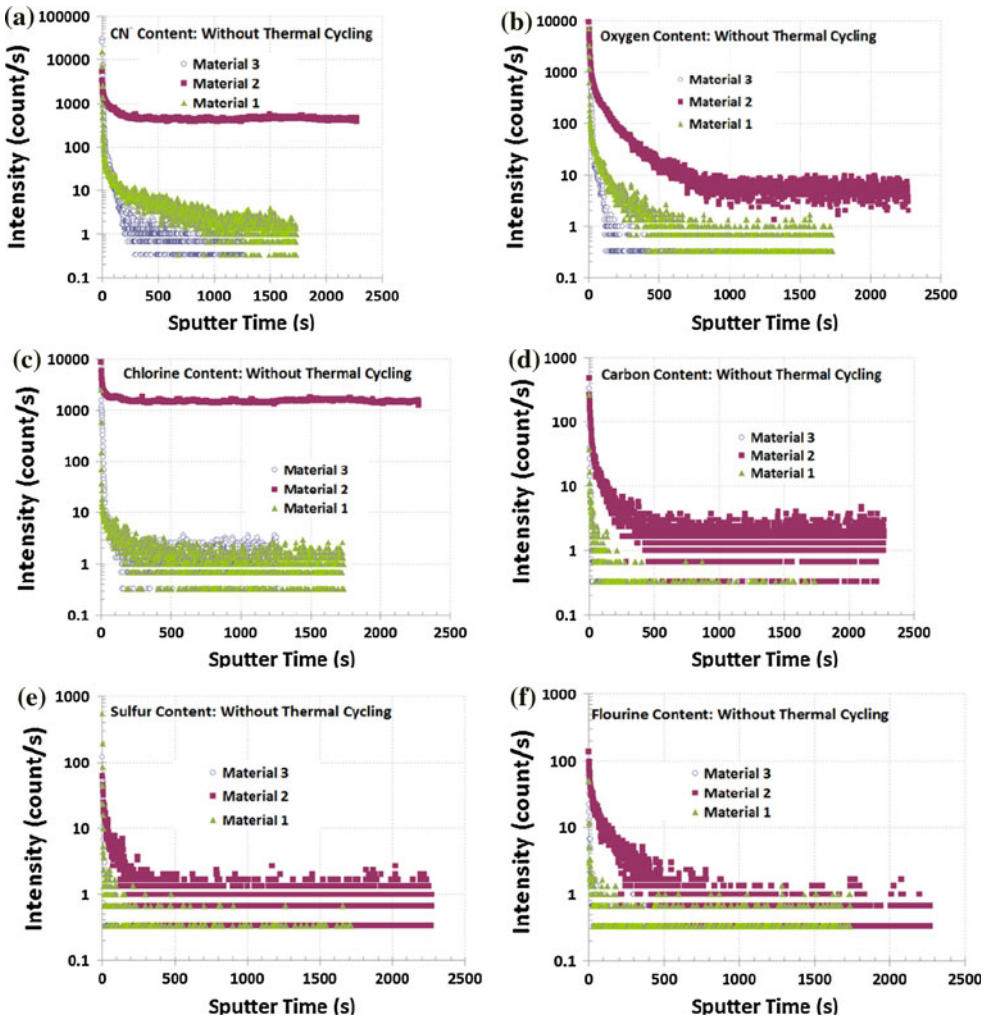

Fig. 6 TOF-SIMS plots for the Material 1, Material 2, and Material 3 Cu-films before thermal cycling. The detected elements are **a** Cyanide fragment, **b** Oxygen, **c** Chlorine, **d** Carbon, **e** Sulfur, and **f** Fluorine

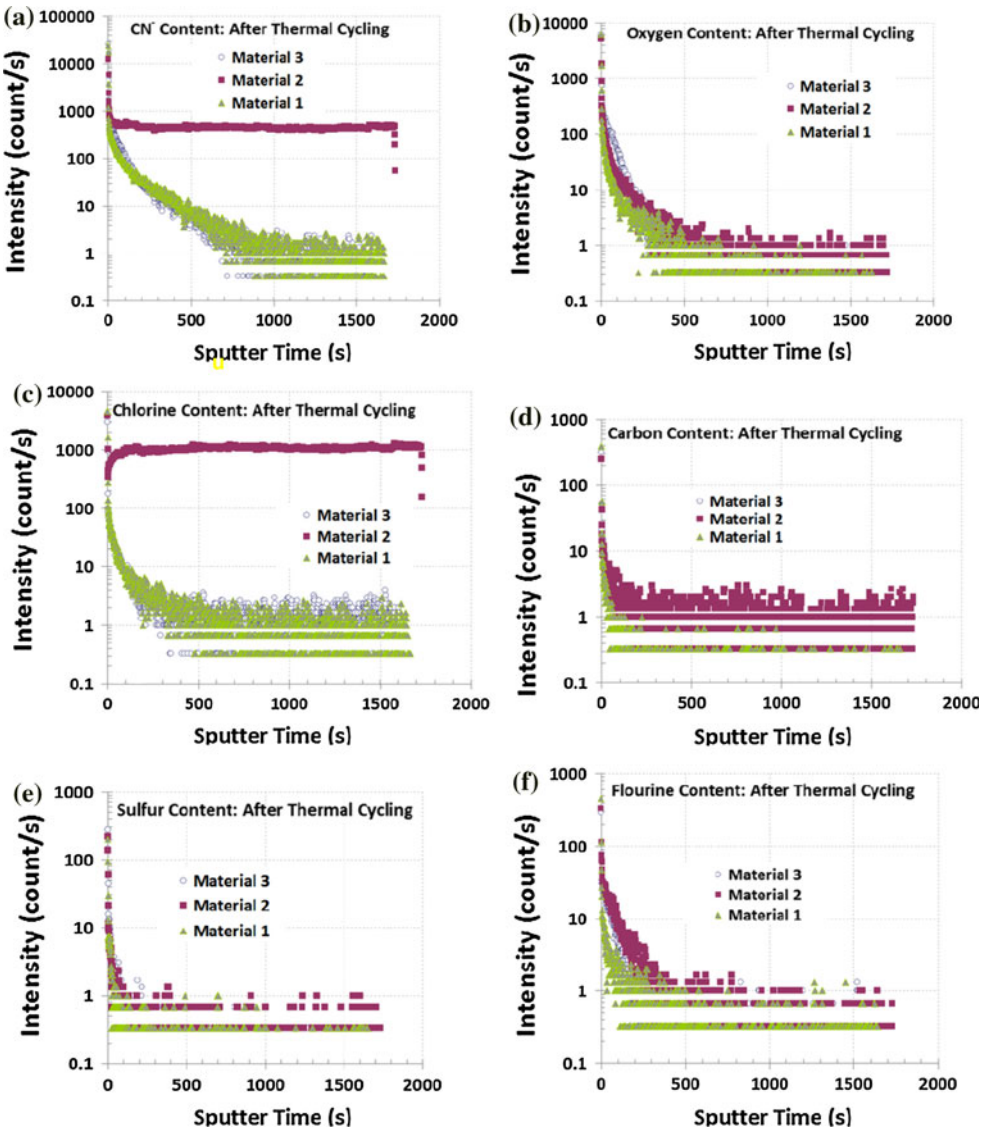

Fig. 7 TOF-SIMS plots for the Material 1, Material 2, and Material 3 Cu-films after thermal cycling. The detected elements are **a** Cyanide fragment, **b** Oxygen, **c** Chlorine, **d** Carbon, **e** Sulfur, and **f** Fluorine

in the lower observed intensity of these elements. This outgassing phenomenon has also been reported by Liang Yin et al. [22] in their study of electroplated Cu-films. The same is observed for the oxygen content which had an intensity of about 5 counts/s *before* thermal cycling, *after* thermal cycling the intensity is observed to decrease to about 1 count/s. Negligible carbon content is observed both *before* and *after* thermal cycling. This therefore means that the observed variations in the CN^- profiles are linked to nitrogen variations. This incorporated nitrogen in the Material 1 Cu-film can be ascribed to JGB additive (leveler), which is the only component in the solution containing nitrogen [4]. The identified chlorine is from the incorporated chlorine ions added to the electrolyte solution of Cu sulfate, while the carbon content (Figs. 6d, 7d) comes from all the constituent additives.

Thus, it could be concluded that the Material 2 chemistry contained the highest level of impurities as it showed high traces of chlorine, nitrogen, oxygen, and carbon. On the other hand, the Material 3 and the Material 1 Cu-films were observed to show very minimal traces of nitrogen and chlorine, thus, they can be said to be of high-Cu purity.

Microstructural examination of the different Cu-films

Microstructural examinations of the different studied Cu-films were performed. Similar to the TOF-SIMS analysis, two tests were performed on each of the samples; *before* thermal cycling and *after* thermal cycling, so as to capture the effect of thermal cycling on the microstructural evolution of the Cu-films.

Material 1 Cu-film chemistry

Figure 8 shows the FIB images of the microstructure of the Material 1 chemistry *before* and *after* thermal cycling. From Fig. 8a which is the microstructure for the test *before* thermal cycling, non-uniformity in grain size can be observed with high defect density in the form of twins. This suggests that the film has already recrystallized under RT conditions, which is often referred to as self-annealing [7]. During the first thermal cycle, the Material 1 chemistry exhibits an abnormal grain growth pattern. Abnormal grain growth is a growth pattern in which some isolated grains grow at faster rates and annihilate the growth of the surrounding normal grains [23], which leads to some grains being much larger than their neighboring grains.

After thermal cycling (Fig. 8b), the grains are observed to increase in size, with grains sizes much larger than 10 μm, which is larger than the thickness of the film itself. This abnormal grain growth pattern is clearly confirmed by the EBSD studies shown in Fig. 9.

In addition, cavities and voids can be observed along the grain boundaries of the samples *after* thermal cycling. This means that some transport of mass during the heating stage of the thermal cycling process has occurred. This mass transport could occur by coble creep which is a diffusional creep mechanism which occurs through the diffusion of atoms in a material along the grain boundaries that results in a net flow of material and can serve as an accommodation mechanism during sliding of the grain boundaries [24], [25]. In addition to grain boundary sliding, the voids could also have been formed due to the high localized stresses caused by the elastic anisotropy of copper. The discontinuity in elastic properties on crossing grain boundaries can be expected to cause significant localized stresses [26–28].

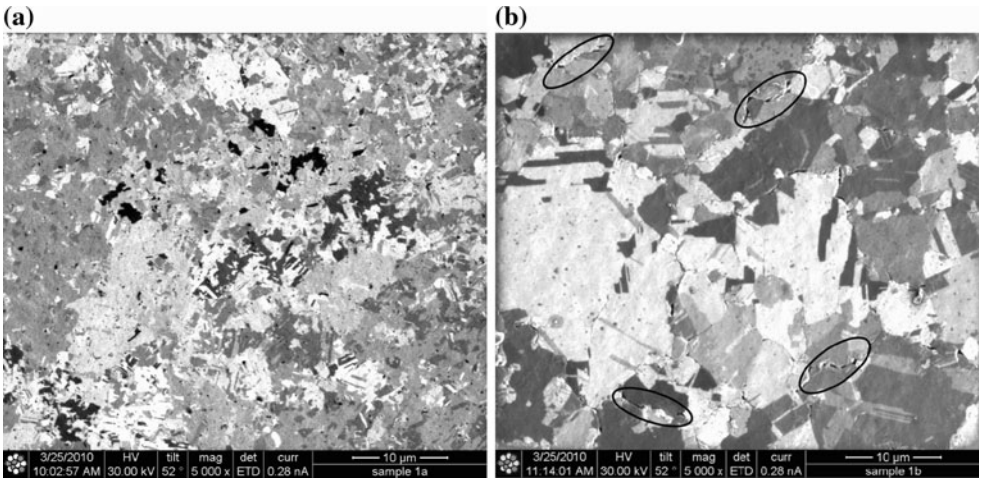

Fig. 8 FIB image of the microstructure of Material 1 Cu **a** *Before* thermal cycling **b** *After* thermal cycling. The highlighted regions are cavities observed at the grain boundaries

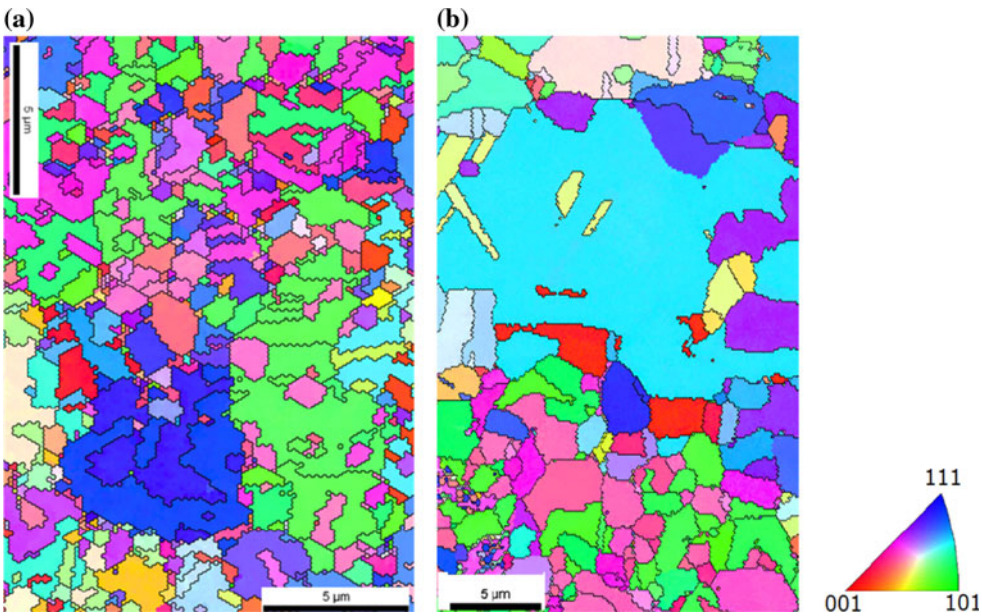

Fig. 9 EBSD image of the microstructural structure of the Material 1 chemistry. **a** *Before* thermal cycling **b** *After* thermal cycling

From the EBSD analysis, the grain size distribution for the two different thermal cycling states (*before* and *after* thermal cycling) are calculated and presented in Fig. 10 below. It is worth noting that for this analysis the twin boundaries were included in the calculation of the grain size distribution. *Before* thermal cycling, the maximum grain size is observed to be less than 3 μm in diameter (see Fig. 10a); however, *after* thermal cycling an increased spread in the grain distribution is observed with a maximum grain size of about 5 μm (see Fig. 10b). An average grain size of 0.58 and 0.81 μm were obtained, respectively, *before* and *after* thermal cycling.

Material 3 Cu-film chemistry

For the Material 3 Cu-film (see Fig. 11), *before* thermal cycling the grain structure is observed to have high density defects which are much similar to the Material 1 Cu-film. However, the grains can be observed to be much more uniformly distributed across the film surface. *After* thermal cycling, the grains of the film are observed to grow with very visible twin boundaries, but less defect density in comparison to the film structure *before* thermal cycling. In addition, their grain sizes can be seen to be uniformly distributed, thus, it could be said that it exhibits a normal grain growth pattern. This is a grain growth pattern which is basically driven by the reduction of the total grain boundary area and the corresponding reduction in the total grain boundary energy that accompanies the area decrease.

This is a common growth pattern observed in bulk materials [23], [29]. The grain distribution function is monomodal. This is confirmed by the EBSD images shown in Fig. 12. From this figure, it can be observed that a more or less random grain orientation distribution is observed for both thermal cycling states. In addition, the uniformity in the grain size can be observed to increase upon thermal cycling, as Fig. 12a is observed to show a more random grain size distribution than the Fig. 12b, *after* the sample has been thermally cycled.

The grain size distribution of Material 3 is presented in Fig. 13. It is observed that upon thermal cycling, the maximum grain size increases from about 4 μm *before*

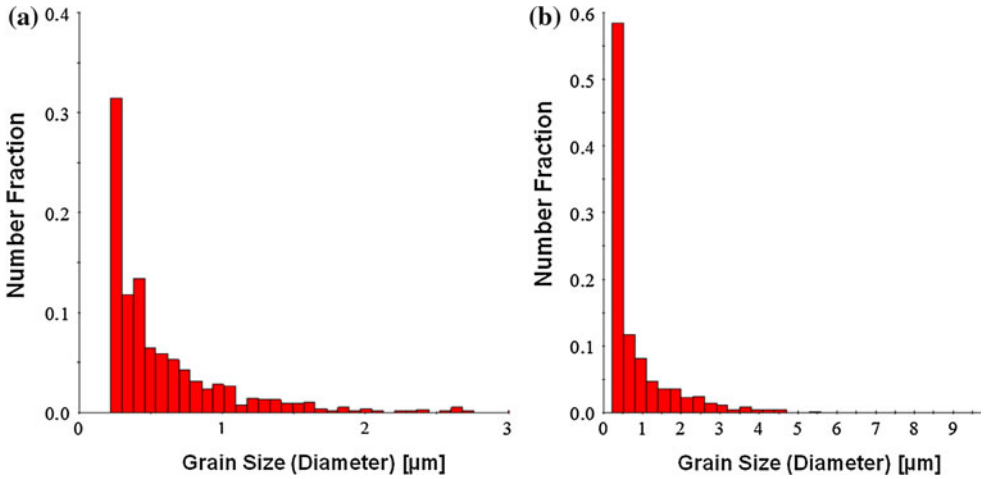

Fig. 10 Grain size distribution EBSD images of the microstructure of the Material 1 Cu-film. **a** *Before* thermal cycling **b** *After* thermal cycling

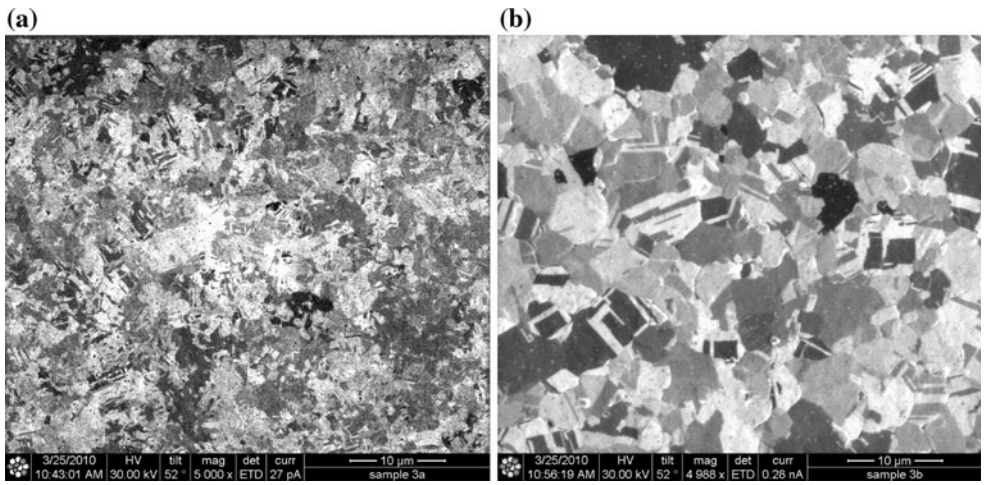

Fig. 11 FIB image of the microstructure of Material 3 Cu-film **a** *Before* thermal cycling **b** *After* thermal cycling

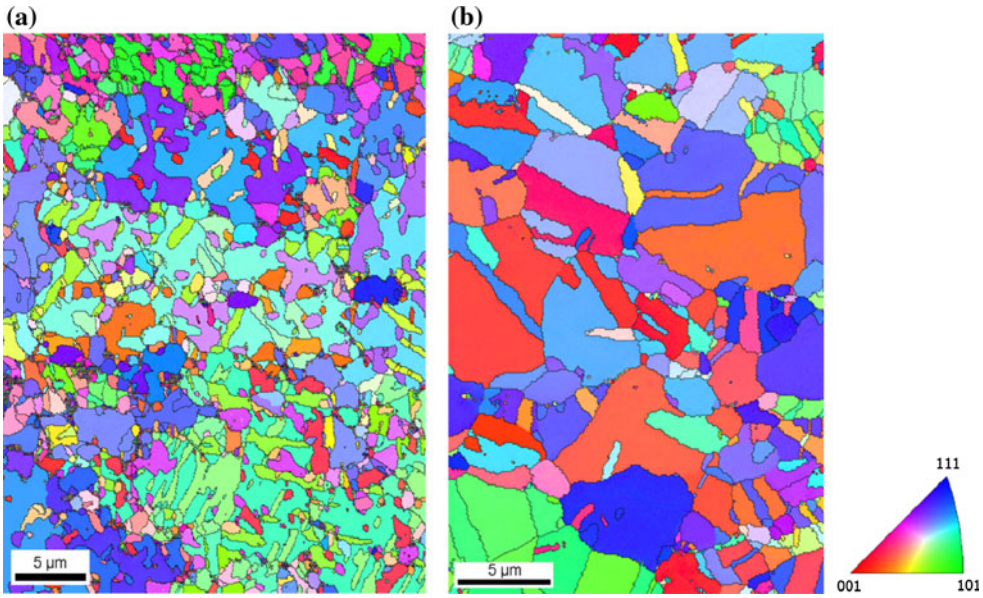

Fig. 12 EBSD images of the microstructure of the Material 3 Cu-film. **a** *Before* thermal cycling **b** *After* thermal cycling

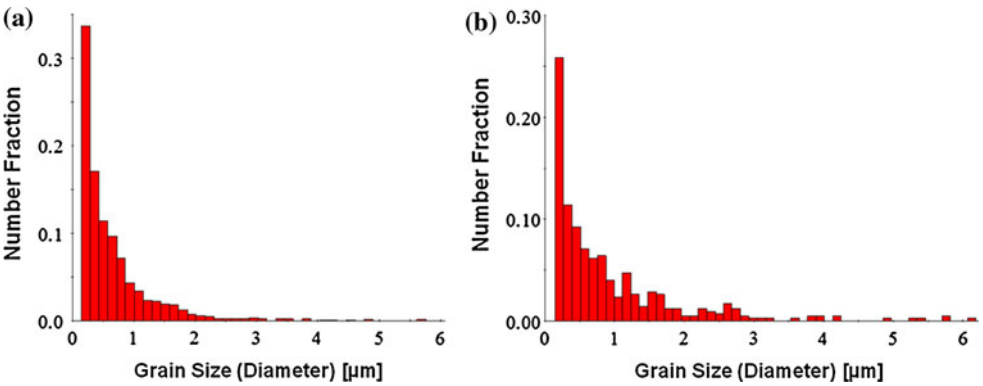

Fig. 13 Grain size distribution EBSD images of the microstructure of the Material 3 Cu-film. **a** *Before* thermal cycling **b** *After* thermal cycling

thermal cycling (Fig. 13a) to more than 6 μm *after* thermal cycling (see Fig. 13b). In addition, a larger spread in the grain size distribution is observed *after* thermal cycling (Fig. 13b), this is due to the growth of the grains upon thermal cycling.

An average grain size of 0.63 and 0.91 μm were obtained, respectively, *before* and *after* thermal cycling.

Material 2 Cu-film chemistry

The FIB images of the microstructure of the Material 2 *before* and *after* thermal cycling are illustrated in Fig. 14. The film is observed to be rough, having a very fine grain structure, much finer than that of the Material 1 and the Material 3 Cu-films.

The grains are observed to be uniformly distributed across the surface of the film. *After* thermal cycling, it can be seen in Fig. 14b that very little grain growth is observed in the grains. The reason for this inhibited growth of the Material 2 Cu-film will be discussed in Sect. Discussion. Also, from the morphology of the grain structure it could be observed that the grains after thermal cycling are uniformly distributed, thus, exhibiting a normal grain growth pattern. No visible voids could be found in the film both *before* and *after* thermal cycling.

However, due to the roughness and the small size of the grains of the Material 2 Cu-film, EBSD analysis could not be performed, as the used EBSD tool has a resolution limit of 100 nm.

Nano-indentation results

Nano-indentation measurements were performed on the three different electrodeposited Cu chemistries. For each of the Cu-films, nano-indentation measurements were done *before* and *after* thermal cycling. From the indentation measurements, the elastic modulus and the hardness values were extracted as a function of the indentation depth. This study is performed using a nano-indenter XP system (MTS

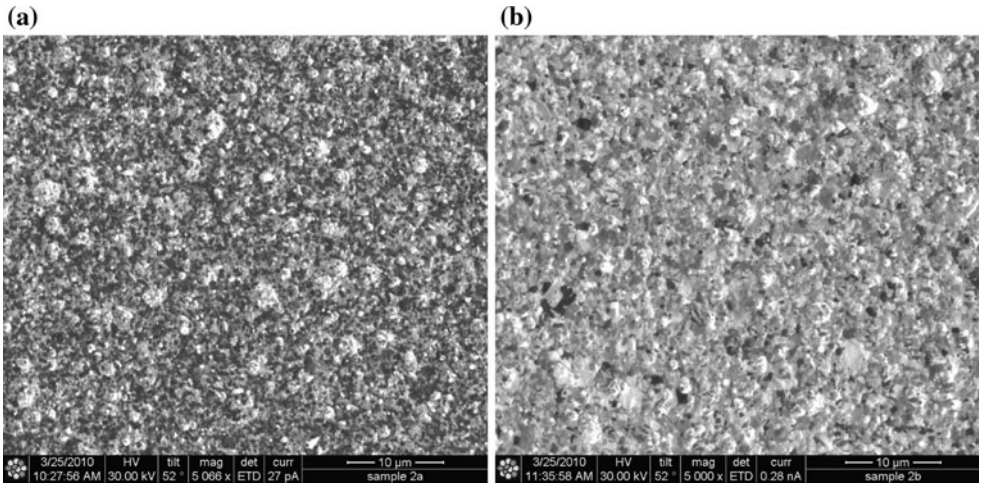

Fig. 14 FIB image of the microstructure of Material 2 Cu-Film **a** *Before* thermal cycling **b** *After* thermal cycling

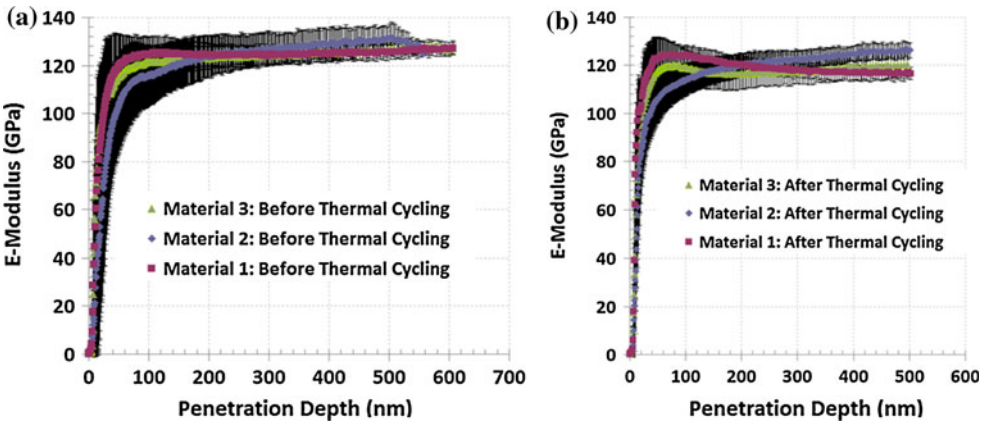

Fig. 15 Plot of the elastic modulus of the different Cu-films as a function of the penetration depth of the indenter tip. **a** *Before* thermal cycling **b** *After* thermal cycling

Systems Corporation) with dynamic contact module (DCM) and continuous stiffness measurement (CSM) option under constant strain rate condition of 0.05/s. For this experiment, 40 indentation repetitions were performed so as to have a meaningful statistics.

Elastic modulus measurements

Figure 15 shows the elastic modulus results *before* and *after* thermal cycling for the three different Cu-films. A similar trend in the measured elastic modulus as a function of the penetration depth is observed for the different electrodeposited Cu-films.

The elastic modulus values are observed to increase steadily and saturated after a penetration depth of about 80 nm. The reason for this initial variation is related to the surface roughness of the Cu-films, as the indenter tip initially does not make a proper contact with the film, leading to the variation in the measured elastic modulus. However, after a penetration depth above 80 nm the measured elastic modulus remained constant. The elastic modulus data are extracted from a penetration depth of 200 nm for the three Cu-films *before* and *after* thermal cycling. The results are presented in Fig. 16. From this graph it seems that the recorded average values for the indentation measurements *before* thermal cycling are higher than those *after* thermal cycling; however, it could be observed that they show an

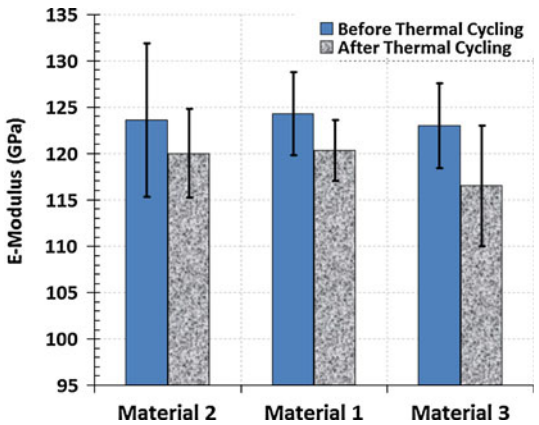

Fig. 16 Graphical representation of the extracted elastic modulus data at a penetration depth of 200 nm

overlapping error bar. This means that no significant change in elastic modulus is observed for the different Cu-films for the different tested thermal treatment states. An average "across board" elastic modulus value of about 121 GPa can be assumed for all the Cu-films.

Hardness measurement

From Fig. 17, it could be observed that after a full contact has been made by the indenter tip with the sample at a depth of about 50 nm that the hardness is found to decrease with indentation depth until about a depth of 400 nm where it is observed to saturate for all Cu-films and test conditions (except for the Material 2 Cu-film *before* thermal cycling). This observed higher hardness at lower indentation depth is due to indentation size effect [30]. It is an artifact caused by the high strain gradient initiated by the sharp indenter tip as it penetrates the film. This strain gradient leads to localized strain hardening which is observed as an increase in hardness. However, as the indenter tip penetrates further, the localized strain gradient decreases leading to a constant measured hardness. For this reason, the hardness results are extracted from a depth of 450 nm, since the hardness results are constant above a penetration depth of 400 nm. The results are presented in Fig. 18, and a clear difference in the hardness of the Cu-films for the different thermal treatment states is observed. The Material 2 Cu-film is observed to show higher hardness values than the Material 1 and the Material 3 Cu-films, having a value of 2.5 ± 0.18 and 1.5 ± 0.5 GPa *before* and *after* thermal cycling, respectively. While for the same thermal treatment condition, the Material 1 and the Material 3 Cu-films are observed to have similar hardness values of about 1.4 and 1.1 GPa, respectively, *before* and *after* thermal cycling as is illustrated in Fig. 18. This therefore means that the measured hardness values for the different Cu-films decreased upon thermal cycling.

This is due to the increase in the grain size of the Cu-films upon thermal cycling as could be observed in Figs. 8b, 11b, and 14b, respectively, for the Material 1, Material 3, and the Material 2 Cu-films. This is in accordance with the Hall–Petch relation which states that the yield stress of a material is proportional to the $d^{-0.5}$,

$$\sigma_y = \sigma_i + kd^{-0.5} \tag{5}$$

where σ_y is yield stress, σ_i is intrinsic stress in the film, k is the Hall–Petch coefficient, and d is the average grain size, and the yield stress can be taken as 1/3 of the hardness value [31, 32].

This decrease in hardness values with respect to grain size is expected, since hardness is a measure of a materials' resistance to flow, thus, local substructural effects such as the size of the grains are expected to have an influence on the measured hardness values.

Therefore, the reason why the Material 2 Cu-film showed a much higher hardness values both *before* and *after* thermal cycling than the other Cu-films is related to their finer grain size.

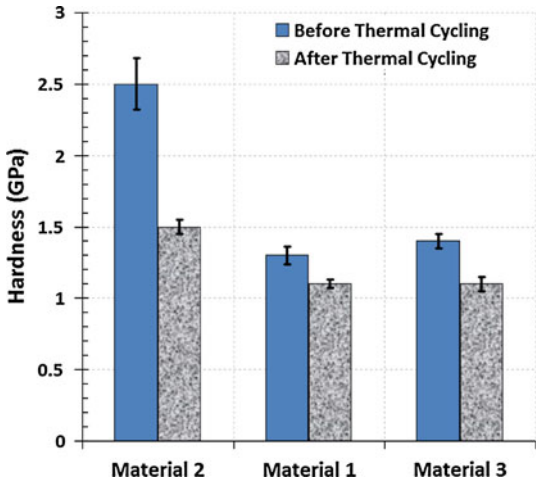

Fig. 18 Graphical representation of the extracted hardness data at a penetration depth of 450 nm

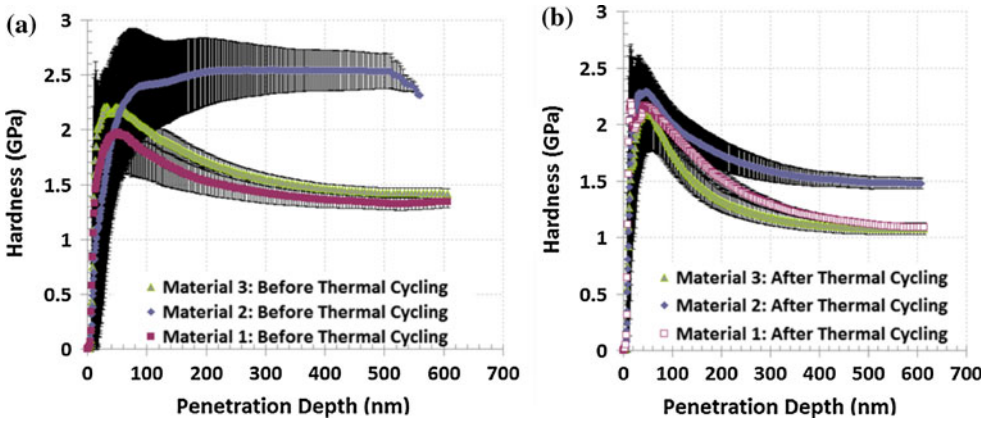

Fig. 17 Plot of the hardness of the different Cu-films as a function of the penetration depth of the indenter tip. **a** *Before* thermal cycling **b** *After* thermal cycling

Discussion

Based on the additional analysis discussed in Sects. TOF-SIMS analysis, Microstructural examination of the different Cu-films, and Nano-indentation results, the differences witnessed in the stress–temperature response of the different Cu-films illustrated in Figs. 3, 4, and 5 can be explained in more detail.

The Material 1 and the Material 3 Cu-films showed similar thermo-mechanical behavior as could be observed in their stress–temperature curves presented in Figs. 3 and 4. This similarity in behavior is due to their equivalent purity level. From the TOF-SIMS results presented in Figs. 6 and 7, it can be observed that both Cu-films have comparable levels of impurities, thus resulting in the witnessed similarity in their thermo-mechanical behavior.

On the other hand, the Material 2 is found to witness a high maximum tensile stress of about 650 MPa, which is more than three times the stress observed in the other Cu-films; the Material 1 and the Material 3 Cu-films. In addition, after the initial thermal cycle it is observed to behave somewhat elastically, with a characteristic narrow hysteresis loop, which is not observed in the Material 1 and the Material 3 Cu-films as they exhibited an elastic–plastic response with a much larger hysteresis loop area. The explanation for this difference in thermo-mechanical behavior lies in the mechanical, microstructural analysis, and the chemical composition analysis (TOF-SIMS) presented in Sects. TOF-SIMS analysis, Microstructural examination of the different Cu-films.

The microstructural analysis presented in Fig. 14 showed that the grain size of the Material 2 Cu-film is finer than the other studied Cu-films. Even after thermal cycling, grain growth is observed to be very minimal (Fig. 14), unlike the grains of other Cu-films that grew extensively larger upon thermal cycling (Figs. 8b, 11b). This limited growth of the grains is caused by the high impurity content of the Material 2 chemistry, which contained high levels of impurities such as chlorine, nitrogen, oxygen, and carbon (see Figs. 6, 7) *before* and *after* thermal cycling. Therefore, since the dynamics of grain growth and recrystallization in electroplated Cu are closely related to the impurities that are trapped in the deposit during plating [10], they will affect the thermo-mechanical behavior of electroplated Cu-films. The mechanism for the influence of impurities observed in the Material 2 Cu-film can be explained by Zener pinning [33], which is a phenomenon in which second-phase particles impede the grain growth of the major phase by pinning the motion of their grain boundaries [34] and/or by solute drag effects. This means that the analyzed impurities observed in the Material 2 Cu-film (see Figs. 6, 7) gets distributed along the grain boundaries of the Cu-film as second-phase particles or as individual atoms, inhibiting the free growth of the grains by pinning their grain boundaries. These impurities also act as obstacles to the free movement of dislocations, which limits the relaxation of stress, resulting in a high stress build up in the film as can be observed in Fig. 5. This explains why the Material 2 Cu-film showed limited plastic deformation, thus, the narrow hysteresis loop and a high stress that is three times higher than the other studied Cu-films.

While for the Material 1 and Material 3 Cu-films, since their impurity contents are negligible (see Figs. 6, 7), their grains have much more freedom to grow and relax the built up thermal stresses since there is a limited resistance to the movement of dislocations and to grain growth, as they do not have any significant second-phase particles. This results in the lower maximum stress of about 200 MPa and the larger hysteresis loop observed in Figs. 3 and 4, respectively, for the Material 1 and the Material 3 Cu-films. Therefore, higher impurity content resulting from electroplating additives leads to a much larger inhibition of the free growth of the grains, thus, the formation of smaller grains, as has been also observed in the study of Zhang et al. [10].

Implications of residual stress in Cu–TSV

Studies have been reported previously by the authors in [12] in which Micro Raman spectroscopy was used to measure the stress in a wafer containing Cu–TSVs. It was found that the stress in silicon is induced by the surrounding Cu–TSV, and the measured stress scaled with the applied annealing treatment temperature that the test samples were subjected to. This is because increase in thermal strain is proportional to the change in temperature [11–13], which results in an increase in stress. Thus, from this study, we could conclude that stresses in Si are induced by the presence of Cu–TSVs and that the induced stresses in Si increase with the residual stress in Cu–TSV.

In addition, electrical measurement studies performed by [35] on Cu–TSV containing wafers after they received prior thermo-mechanical treatments showed that the presence of Cu–TSVs resulted in a significant change in the integrated CMOS devices. The magnitude of this variation is found to be directly dependent on the proximity of the integrated CMOS devices from the Cu–TSV. Similar trends were also observed by [36], as these studies were achieved on the advanced 65 nm CMOS technology platform. However, studies performed using the much older 130 nm CMOS technology platform [37] showed no influence of the Cu–TSV on transistor performance.

This could also be extended to the thermo-mechanical behavior of the used Cu electroplating chemistry. Therefore, TSVs filled using the Material 2 chemistry, which

showed higher residual stresses (Fig. 5), are anticipated to result in a much higher induced stresses in Si, thus, higher potential impact on integrated transistors, than the Material 1 or the Material 3 Cu chemistries. Therefore, before the selection of the electrodeposition chemistry to be used for the filling of TSVs, the thermo-mechanical behavior of such Cu electrodeposition chemistry should be given a thought.

Conclusions

The Material 2 Cu-film is found to have a residual stress that is more than three times that of the other studied Cu-films; Material 1 and the Material 3 Cu-films. In addition, it is observed to exhibit a limited plastic deformation, as it showed a very narrow hysteresis loop with no stress plateau after the first cycle, while the other Cu-films were found to show a characteristic elastic–plastic response to the applied temperature. This unexpected behavior in the Material 2 is attributed to the presence of high levels of impurities such as chlorine, nitrogen, and oxygen in the electrodeposition bath. These impurities get distributed within the grain boundaries and by Zener pinning and/or by solute drag effects, prevent the free growth of their grains, as they also inhibit the free movement of dislocations. Hence, they limit stress relaxation, which leads to the observed higher stress in the film in comparison to the other studied films.

Microstructural analysis of Material 1 revealed an abnormal grain growth pattern, in which the sizes of their grain were unevenly distributed. After thermal cycling voids were observed along the grain boundaries of the Material 1. The formed voids are attributed to Coble diffusional creep mechanism, where mass transport occurs along the grain boundaries and to anisotropic elastic property difference between neighboring grains, which result in high localised stresses, which aids void formation. Thus, the voids are formed as a stress relaxation mechanism. However, for the Material 2 and the Material 3 Cu-films, they are observed to have an evenly distributed grain structure both *before* and *after* thermal cycling without any visible void formation, and they show a normal grain growth pattern.

In previously performed studies by micro Raman spectroscopy it was found that the measured stress in Si is caused by the presence of Cu–TSVs. This means that higher residual stress in the Cu–TSV will result in an increase in the induced stresses in the Si, which could influence the characteristics of transistors in close proximity to the Cu–TSVs.

Therefore, the choice of Cu electrodeposition solution should not be limited only to the achievement of a void free Cu–TSV, they should also be judged based on their thermo-mechanical behavior, as it could have reliability consequences.

Acknowledgement The authors would like to thank Chris Drijbooms and Hugo Bender of the MCA group at IMEC for the FIB results presented in this article.

References

1. Lühn O et al (2009) Electrochim Acta 54:2504
2. Lühn O et al (2009) Electrochem Solid-State Lett 12(5):D39
3. Lühn O et al (2008) In: Proceedings of the 58th electronics components and technology conference (ECTC), Orlando, pp 866–870
4. Lühn O et al (2009) PhD Thesis, Katholieke Universiteit Leuven, Belgium, pp 143–151
5. Van Bavel M et al (2008) Future FAB Int 27(7):112
6. Dixit P et al (2006) J Electrochem Soc 153(6):G552
7. Okoro C et al (2010) J Micromech Microeng 20:045032
8. Changdong G et al (2009) J Micromech Microeng 19:065011
9. Luhua X et al (2007) Appl Phys Lett 90:033111 3 pp
10. Zhang W et al (2005) In: MRS conference proceedings, p 347
11. Okoro C et al (2007) In: Proceedings of the electronics components and technology conference (ECTC), Reno, p 249
12. Okoro C et al (2008) In: Proceedings of the 11th international interconnect technology conference, San Francisco, p 16
13. Van De Plas G et al (2010) Design Issues and Considerations for Low-Cost 3D TSV IC Technology ISSCC 2010, p 148
14. Okoro C et al (2010) In: Proceedings of the American Institute of Physics Conference, vol 1300, Stress-Induced Phenomena in Metallization: 11th International Workshop, p 214
15. Van Olmen J et al (2008) 3D stacked IC demonstrator using hybrid collective die-to-wafer bonding with copper through silicon vias (TSV). IEEE IEDM, San Francisco, p 603
16. Huyghebaert C et al (2010) In: Proceedings of the 60th electronics components and technology conference, Las Vegas, p 1083
17. Janssen GCAM et al (2009) Thin Solid Films 517(6):1858
18. Wyko Surface Profilers Technical Reference Manual, p 1-1-14
19. Thouless MD (1995) Annu Rev Mater Sci 25:69
20. Shen YL et al (2003) J Vac Sci Technol B 21(4):1258
21. Gardner DS et al (2008) IEEE Trans Electron Devices 35(12): 2160
22. Yin L et al (2009) In: Proceedings of the 59th electronic components and technology conference, San Diego, p 406
23. Vanstreels K (2007) PhD Thesis, University of Hasselt, Diepenbeek, Belgium
24. Kobrinsky MJ et al (2001) J Appl Phys 89(1):91
25. Korhonen MA et al (1991) J Appl Phys 70:6774
26. Chidiambarrao D et al (1997) Metall Mater Trans A 28(12):2515
27. Su P et al (1999) In: Kraft O, Arzt E, Volkert CA, Ho PS, Okabayashi H (eds) In: Proceedings of the American institute of physics, 5th worshop on stress-induced phenomena in metallization, New York, p 298
28. Shaw TM et al (2002) In: Baker SP et al (eds) In: Proceedings of the American institute conference, vol 612, 6th workshop on stress-induced phenomena in metallization, p 177
29. Atkinson HV (1988) Acta Metall 36(3):469
30. Pharr GM et al (2010) Annu Rev Mater Sci 40:271
31. Volinsky AA et al (2001) Mater Res Symp 649:Q5.3.1
32. Tabor D (1951) The hardness of metals. Claredon Press, United Kingdom, p 174
33. Harper JME et al (1999) J Appl Phys 84(5):2516

34. El-Khozondar R et al (2006) Egypt J Solids 29(1):347
35. Mercha A et al (2010) Comprehensive Analysis of the Impact of Single and Arrays of Through Silicon Vias Induced Stress on High-k/Metal Gate CMOS Performance. International Electron Devices Meeting (IEDM, San Francisco, p 2.2.1
36. Mercha et al (2010) Impact of thinning and through silicon via proximity on high-k/metal gate first CMOS performance. VLSI Technology, Honolulu, p 109
37. Yang Y et al (2010) International Interconnect Technology Conference (IITC), Burlingame, p 1